European Polymer Journal 165 (2022) 110997

Contents lists available at ScienceDirect

European Polymer Journal

journal homepage: www.elsevier.com/locate/europolj

# New way to obtain the poly(L-lactide-*co*-D,L-lactide) blend filled with nanohydroxyapatite as biomaterial for 3D-printed bone-reconstruction implants

Sara Targonska [a], Monika Dobrzynska-Mizera [b,*], Marta Wujczyk [a], Justyna Rewak-Soroczynska [a], Monika Knitter [b], Katarzyna Dopierala [c], Jacek Andrzejewski [b], Rafal J. Wiglusz [a,*]

[a] Institute of Low Temperature and Structure Research, PAS, Okolna 2, PL-50-422 Wroclaw, Poland
[b] Institute of Materials Technology, Polymer Division, Poznan University of Technology, Piotrowo 3, 61-138 Poznan, Poland
[c] Institute of Chemical Technology and Engineering, Poznan University of Technology, Berdychowo 4, 60-965 Poznan, Poland

ARTICLE INFO

*Keywords:*
Poly(L-lactide-*co*-D,L-lactide)
Nanohydroxyapatite
Biocomposite
Co-rotating twin-screw extrusion
Bone-fixation material

ABSTRACT

A novel, bone-reconstruction dedicated polymeric-nanohydroxyapatite material has been prepared for 3D-printed implant. The composites of poly(L-lactide-*co*-D,L-lactide) (PLDLLA) and nanosized hydroxyapatite were prepared by a co-rotating twin-screw extrusion. Structural properties of the filler and polymeric blends were characterized by XRD (X-ray Powder Diffraction), SEM (Scanning Electron Microscopy), and EDS mapping (energy dispersive spectroscopy), FT-IR (Fourier-transformed infrared spectroscopy), and NMR (Nuclear Magnetic Resonance) technics. Molar masses of the composites at various preparation steps were also investigated. The structural studies and thermogravimetric analysis proved a successful preparation of the nanohydroxyapatite and its nanocomposites. Mechanical results in conjunction with density values, reported as close to human bone, evidenced usability of this novel material for internal bone fixation implant. Contact angle analysis showed favored growth of tissue on the biocomposite containing 10 wt% of the filler. The PLDLLA-based composite can be an excellent candidate for bone reconstruction implants due to their superior mechanical properties, bioactivity, and complete resorbability.

## 1. Introduction

In the field of orthopedics and bone surgery, commercially available bioresorbable solutions are based on polymers and co-polymers of lactic acid, ethane-1,2-diol (ethyl glycol), or chitosan (poly-(D)-glucosamine) [1–4]. Polylactides are of particular interest due to their bioresorbability, ease of processing, and shaping by a number of industrial methods, as well as mechanical strength. Poly(lactic acid) may be formed as two different stereoisomers: left poly(L-lactic) acid (PLLA) and right poly(D-lactic) acid (PDLA) [5–8]. The PLLA has been used since the early 1990s as "the first generation" bioresorbable material [9]. However, the PLLA is resistant to hydrolysis; thus, its complete resorption in *in vitro* tests does not occur within the first two years of implementation due to its crystallinity and hydrophobicity [10,11]. Such behavior may cause medical problems including inflammatory or late-degradation tissue responses [12–14]. To overcome these issues, "the second generation" materials have been designed, namely co-polymers of PLLA and PDLA, whose properties and degradation rate vary with the composition.

The physicochemical and mechanical properties of these co-polymers can be further tailored by the addition of bioactive inorganic fillers [15,16]. Their introduction enables achieving desired kinetics of degradation, resorption, and mechanical strength of a polymeric matrix [17]. Nanosized synthetic hydroxyapatite (nHAp) is an example of such a filler. The nHAp crystals are similar to the natural structure of bone-building apatite in composition, size, and morphology. Hence, it is widely employed for hard tissue repair in orthopedic surgery and dentistry [18]. Apatite-like compounds crystallize in the hexagonal crystal structure. The calcium hydroxyapatite molecule is made up of ten calcium atoms, six phosphate groups, and two hydroxyl groups, giving a molecule with the summarized formula $Ca_{10}(PO_4)_6(OH)_2$ [19–21].

Many reports on bioactive/resorbable composites of hydroxyapatite

* Corresponding authors.
*E-mail addresses:* monika.dobrzynska-mizera@put.poznan.pl (M. Dobrzynska-Mizera), r.wiglusz@intibs.pl (R.J. Wiglusz).

https://doi.org/10.1016/j.eurpolymj.2022.110997
Received 15 November 2021; Received in revised form 28 December 2021; Accepted 2 January 2022
Available online 6 January 2022

filler and PLLA matrix can be found [9,22–25]. These formulations are reported as the "third generation materials". It has been proved that in the early stage of bone tissue growth, the composites containing more than 5% w/w of hydroxyapatite exhibit higher absorption of protein surface. Such materials may be applied in bone grafting, including maxillofacial surgery, as they possess sufficient mechanical potential and bioactive, osteoconductive/bioresorbable characteristics [9]. However, it should be noted that the PLLA used until now to produce such implants fully disintegrates within the human body after 4 years, while most hydroxyapatite particles are replaced by bone after 5.5 years [9]. This long-term resorption causes complications related to significant inflammatory and late-degradation tissue responses and discomfort when using an implant under fragile skin (e.g., near the facial skin areas), due to an increase in implant volume caused by overbuilding fibrous tissue. In this case, the "next-generation material" has been developed and characterized in our laboratory. The co-polymer of L-lactide and DL-lactide (PLDLLA) was used together with nanosized hydroxyapatite to engineer bioresorption rate/speed and tailor mechanical strength and bioactivity. To the best of our knowledge, different PLLA-based formulations have been widely studied and utilized in medical applications [25]. However, such a composition has not been reported yet.

Apart from in-depth study on implant composition upon design stage, it is also essential to consider its surface in terms of microbial colonization [26]. Site infections are a major cause of post-surgical complications such as extended hospitalization, deterioration in recovery, or even implantation failure [26]. Among the most reported implant-infecting bacteria are Gram-positive and Gram-negative species. However, most infections are caused by *Staphylococcus aureus* and *Staphylococcus epidermidis*. Less frequent are *Streptococcus* spp. and *Enterococcus* spp. and Gram-negative species, like *Pseudomonas aeruginosa*, *Escherichia coli,* and *Klebsiella pneumoniae* [27]. Initially, bacterial cells reversibly adhere to the implant surface, and after some time, the adhesion becomes irreversible, finally leading to the formation of mature biofilm [26]. Biofilm is hard to eradicate because the antibiotic susceptibility to bacteria is decreased. Hence, it is crucial to determine the tendency of the material surface to be settled by specific species of bacteria and prevent it from a bacterial infection especially in the early stages of the medical treatment by providing aseptic conditions during all procedures.

In the presented work, the characterization of physicochemical properties and mechanical behavior of the PLDLLA-based compositions modified with nanosized hydroxyapatite as a filler as well as bacterial adhesion to the material surface was discussed. Large-scale industrial processing methods were employed to enable manufacturing of this innovative material. The Authors have also applied for the patent in the Patent Office of the Republic of Poland to secure the innovative, resorbable compositions for medical applications [P.437485].

## 2. Experimental

### 2.1. Materials

A commercial PLDLLA (Purasorb, L-lactide/DL-lactide copolymer, ratio: 80/20) was kindly supplied by Syntplant sp. z o.o. (Poland). The nanohydroxyapatite was synthesized in the Institute of Low Temperature and Structure Research of the Polish Academy of Science, as detailed below. The nanofiller was used to prepare PLDLLA-based composites with wt.% ratio: 10/90 and 20/80 herein: 10-nHAP/PLDLLA and 20-nHAp/PLDLLA, respectively.

### 2.2. Bacterial strains

Microbial adhesion was tested using a broad panel of bacterial strains: Gram-positive *Staphylococcus aureus* ATCC 6538, *Staphylococcus epidermidis* ATCC 14990, Enterococcus *faecalis* ATCC 29212, *Enterococcus faecium* ATCC 6057, and Gram-negative *Pseudomonas aeruginosa* ATCC 27853, *Escherichia coli* ATCC 35218 and *Klebsiella pneumoniae* ATCC 700603. Tested strains have been collected from the Department of Mycology and Genetics, University of Wroclaw and Department of Pathogen Biology and Immunology, University of Wroclaw.

### 2.3. Methods

#### 2.3.1. Synthesis of hydroxyapatite nanopowder (nHAp)

Nanocrystalline hexagonal hydroxyapatite $Ca_{10}(PO_4)_6(OH)_2$ was prepared by a wet chemical precipitation process at T = 90 °C for 1.5 h. Analytical grades of $Ca(NO_3)_2{\cdot}4H_2O$ (99.0% Alfa Aesar) and $(NH_4)H_2PO_4$ (≥99.0% Fluka) have been used. The stoichiometric number of starting materials was separately dissolved in deionized water. Substrates were mixed, and the pH was adjusted to 10 with $NH_3{\cdot}H_2O$ (99% Avantor Poland). The obtained powder was washed with deionized water several times and dried at 80 °C for 24 h. A well-crystallized product was obtained by heat-treating at 450 °C for 3 h, with an increasing step of 1.3 °C/min.

#### 2.3.2. Preparation of nHAp/PLDLLA compositions

Commercial PLDLLA (Purasorb PLDL 8058, L-lactide/DL-lactide copolymer, ratio: 80/20) was kindly supplied by Syntplant sp. z o.o. (Poland). The PLDLLA with an inherent viscosity of 5.8 dl/g, melting temperature of 130 °C, and melt flow rate of 0.7 g/10 min (210 °C; 2.16 kg) was provided in a form of whitish pellet. All materials were dried under vacuum at 50 °C for 24 h, before processing. PLDLLA pellets were mixed with nHAp in a rotary mixer Retsch GM 200 for 3 min at a rotation speed of 2000 rpm. Homogenizing the premixed materials with different nHAp contents (0–20 wt%) was ensured by molten state extrusion with a Zamak co-rotating twin-screw extruder operated at 210 °C and 60 rpm. The extruded rod was cooled in air and pelletized. nHAp/PLDLLA composites containing 10 and 20 wt% of nHAp were prepared. The composites were compression-molded with a Remi-Plast press at a temperature of 210 °C for 3 min, without any pressure applied to complete melting. After this period, a load of about 200 bar was applied for 5 min; then, the samples were air-cooled to room temperature. The square-shaped plates with a dimension of 120x120x1 mm were obtained and cut to get standardized dimension samples for mechanical analysis.

#### 2.3.3. Characterization of nHAp and nHAp/PLDLLA composites

Powder X-ray diffraction pattern was detected by using a PANalytical X'Pert Pro X-ray diffractometer equipped with Ni-filtered Cu Kα1 radiation (Kα1 = 1.54060 Å, U = 40 kV, I = 30 mA) in a range of 2θ from 5 to 80°. The experimental data were juxtaposed with the Inorganic Crystal Structure Database (ICSD) theoretical pattern and analyzed.

FT-IR spectra were evaluated by Nicolet iS10 FT-IR Spectrometer equipped with an Automated Beamsplitter exchange system (iS50 ABX containing DLaTGS KBr detector), Built-in all-reflective diamond ATR module (iS50 ATR), Thermo Scientific Polaris™ and HeNe laser as an IR radiation source. The spectra were detected in the range of 400–4000 $cm^{-1}$ with a frequency resolution of 4 $cm^{-1}$. The nHAp powder was mixed with optically inactive KBr to prepare a pellet. FT-IR spectra of the nHAp/PLDLLA compositions were collected by the ATR module.

The surface morphology of the 10-nHAp/PLDLLA composition sample was observed by scanning electron microscope equipped with energy dispersive spectroscopy FEI Nova NanoSEM 230 equipped with EDS spectrometer (EDAX PegasusXM4) at an acceleration voltage of 18 kV and spot 3.0. Before observations, a layer of gold was sprayed uniformly over the samples.

The molar masses were determined by gel permeation chromatography (GPC) technique using a multiangle light scattering detector (λ = 690 nm) DAWN EOS (Wyatt Technologies) and a refractive index detector Dn-2010 RI from WGE Dr Bures. The analysis was performed in

THF (Tetrahydrofuran) at 35 °C and with a set of columns: guard, PSS 100 Å, PSS 500 Å, PSS 1000 Å, PSS 100000 Å (Polymer Standard Service) using polystyrene standards. The dispersity indexes (D) were calculated according to Equation (1):

$$D = \frac{M_W}{M_N} \quad (1)$$

where D is a dispersity index, $M_W$ is a weight-average molar weight, and $M_N$ is a number average molecular weight.

$^1$H NMR experiments were recorded on a Bruker AvanceTM 600 MHz. Measurements were made in $CHCl_3$ at 298 K.

TGA analyses were performed in the temperature range between 30 and 800 °C, at a heating rate of 10 °C min$^{-1}$, under a nitrogen atmosphere using a Netzsch TG 209 F1 apparatus. The instrument was temperature-calibrated by analyzing six high purity standards (indium, tin, bismuth, zinc, aluminum, and silver). The balance calibrates automatically with an inbuilt calibration set. Samples of approx. 10 mg were placed in ceramic pans. The decomposition onset temperature $T_o$ was determined at the intersection of tangents to two branches of the thermogravimetric curve [28]. The residual mass $m_R$ was evaluated to validate the amount of nanofiller in the composites. Each measurement was preceded by an empty pan run, subtracted from each thermogram to correct from instrumental drift.

The static tensile analysis was carried out by a single-axis extension using a Zwick Roell 10 kN (Germany). The crosshead speed was 1 mm min$^{-1}$ for Young's modulus analysis and 10 mm min$^{-1}$ in the range of plastic deformation. Following ISO 527–1, Young's modulus ($E_t$), tensile strength ($\sigma_m$), and elongation at break ($\varepsilon_b$) were determined [29]. Ten specimens were tested in each case to ensure measurement reproducibility.

A Zwick Roell 10 kN testing machine, equipped with a rounded bending head and a table with two supports, was utilized to carry out the three-point bending tests. The measurements were carried out per ISO 178 at 23 °C and 50 % humidity [30]. The preload of 0.1 MPa was applied. A crosshead speed of 1 mm min$^{-1}$ was set to determine the bending modulus, while the bending strength and deflection arrow were recorded at 10 mm min$^{-1}$. Ten specimens were tested in each case to ensure measurement reproducibility.

Brinell hardness tests were carried out with a Brinell hardness tester KB Prufttechnik Gmbh, model KB150R, as per PN-EN ISO 2039–1:2004 [31]. During the tests, an intender ball with a diameter of 5 mm and 358 N test force were applied. There were tested ten specimens in each case to ensure measurement reproducibility.

The density measurement was determined by the hydrostatic method according to the PN-EN ISO 1183–1 standard [32]. Weighing of the sample in the air was followed by weighting in an immersion liquid being ethyl alcohol. There were tested ten samples in each case to ensure measurement reproducibility. The density was calculated according to Equation (2):

$$\rho = \frac{m_p}{m_{ci} - m_p} \cdot \rho_{ci} \quad (2)$$

where

$\rho$ – sample density [g/cm$^3$],
$m_p$ – sample mass in the air [g],
$m_{ci}$ - sample mass in an immersion liquid [g],
$\rho_{ci}$ - immersion liquid density [g cm$^{-3}$].

The measurements were carried out at a temperature of 23 °C on a laboratory balance with an accuracy of 0.0001 g, equipped with a hydrostatic adapter to determine the solids' and liquids' density.

The contact angle (CA) measurements of compression molded sheets were performed using Theta Lite optical tensiometer (Biolin Scientific, Helsinki, Finland) operating in the sessile drop mode. The contact angle was measured by releasing a 2 μL drop of liquid by an automated dispenser controlled by One Attension software. Water and diiodomethane were used as polar and dispersive liquids, respectively. At least seven drops of each liquid were put on the material's surface, and the average values were calculated. The CA values were used to calculate the surface free energy according to Owens, Wendt, Rabel, and Kaelble (OWRK) approach as per Equation (3) [33]:

$$(1 + cos\theta_i)\gamma_l = 2\left(\sqrt{\gamma_l^d \gamma_s^d} + \sqrt{\gamma_l^p \gamma_s^p}\right) \quad (3)$$

where $\gamma_s$ is the SFE of a solid, $\gamma_l$ is the surface tension of the probe liquid (water or diiodomethane), while p and d mean dispersive and polar components, respectively.

### 2.4. Bacterial adhesion

PLDLLA-based materials were cut into even 1 cm pieces, transferred to a 24-well plate, and sterilized with UV for 20 min. All bacterial strains were incubated overnight on TSA plates (Tripticasein Soy Broth) (Biomaxima, Lublin, Poland) solidified with 2% of Bacteriological LAB-AGAR (Biomaxima, Lublin, Poland) at 37 °C, suspended in the saline to 0.5 McFarland (DENSIMAT, BioMérieux, Marcy-l'Étoile, France) and 10x diluted in TSB medium (Tripticasein Soy Broth) (Biomaxima, Lublin, Poland). 1 ml of bacterial suspensions were transferred to the wells. The plate was incubated with agitation (125 RPM) for 24 h at 37 °C. Then, the materials were extracted, rinsed twice with the saline, transferred into clean wells, and incubated 20 min with the fluorescent kit: SYTO 9 (λexc = 488 nm), propidium iodide (λexc = 543 nm) (each at the concentration of 1 μL/mL) (LIVE/DEAD™ Bac-Light™ Bacterial Viability Kit, for microscopy, Invitrogen™, Thermo Fisher Scientific; Waltham, MA USA). The observation was performed in a confocal microscope with 2× digital magnification (Olympus IX83 Fluoview FV 1200 (Tokyo, Japan), magnification 20×). As a control, clean samples (without bacteria) were observed as well.

## 3. Results and discussion

The nanohydroxyapatite and nHAp/PLDLLA compositions were characterized by X-ray diffraction, and the results are shown in Fig. 1. The diffraction pattern of nHAp corresponds to the theoretical one associated with hexagonal hydroxyapatite structure (ICSD-26204). No additional phases were observed. Therefore, the applied synthesis method led to the development of the crystal phase purity of nHAp. The most intense peaks are located at 26.0, 31.9, 32.2, 33.0, 34.2, 39.9, 46.8, 49.6°. The X-ray diffraction pattern corresponding to the 10-nHAp/PLDLLA and 20-nHAP/PLDLLA compositions does not contain peaks related to the crystalline phase of polylactide as they are usually localized at 16.51° and 18.93° [34]. In the range of small 2theta angles, the high background is associated with the amorphous structure of polylactide. The presence of lines associated with hydroxyapatite structure in the composites confirms that hydroxyapatite structure is resistant to the extrusion process, independently on wt.% in composition. The position of the respective diffraction lines of nHAp remained unchanged in the compositions.

The Fourier-transformed infrared spectra present the vibrational bands related to the hydroxyapatite and polylactide structures (see Fig. 2). The bands correlated with polylactide are marked with the black dotted lines. In contrast, the orange ones indicate vibrations associated with the hydroxyapatite structure. In the spectra of hydroxyapatite itself and nHAp/PLDLLA compositions, the typical vibrational bands related to the hydroxyapatite structure were found. The triply degenerated antisymmetric stretching modes $\nu_3(PO_4^{3-})$ of the phosphate groups are detected at 1043 cm$^{-1}$ and 1095 cm$^{-1}$. The two lines ascribed to the $\nu_4(PO_4^{3-})$ triply degenerated vibrations are located at 566 cm$^{-1}$ and 602 cm$^{-1}$. At the 962 cm$^{-1}$ lines assigned to the symmetric stretching modes

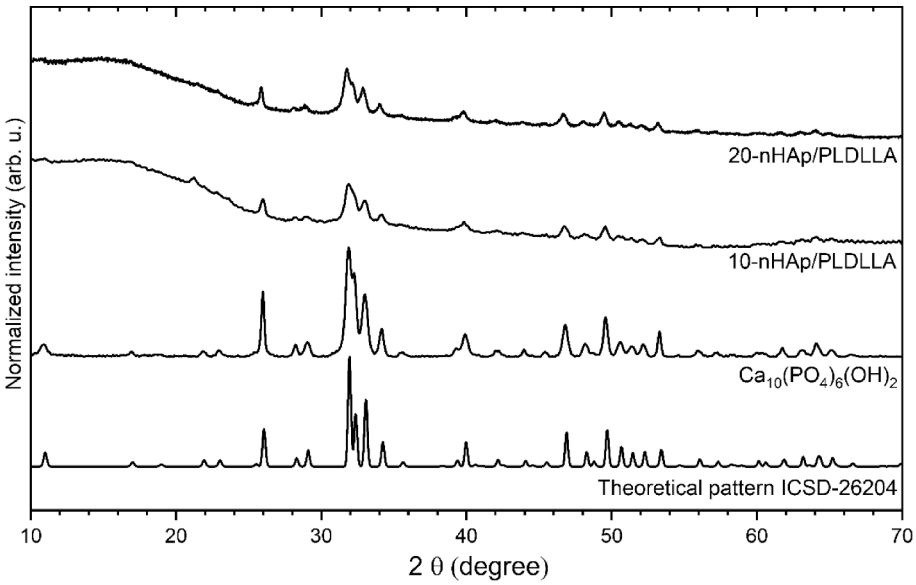


**Fig. 1.** X-ray diffraction pattern of nanohydroxyapatite as well as nHAp/PLDLLA compositions.

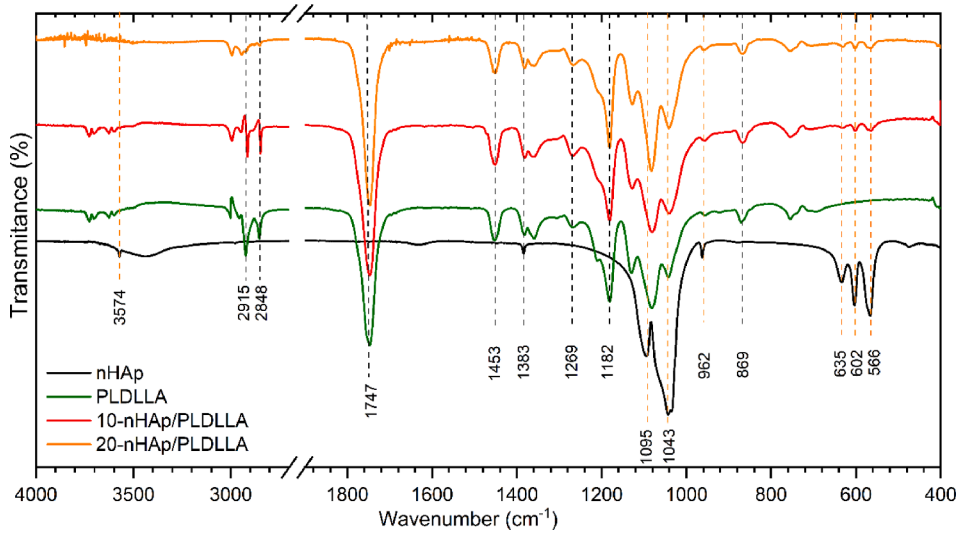


**Fig. 2.** The FT-IR spectra of nanoapatites, PLDLLA as well as nHAp/PLDLLA composition.

$\nu_1(PO_4^{3-})$, the phosphate groups are observed. The two vibrational modes of $OH^-$ groups are scanned at 635 $cm^{-1}$ and 3574 $cm^{-1}$ related to the bending and stretching modes, respectively. The existence of those two modes confirms the presence of hydroxyl groups in nanocrystal structure.

In the spectra of pure polylactide and nHAp/PLDLLA composites, the vibrational modes related to polyester material are detected. The most intense peak at 1747 $cm^{-1}$ is associated with —C═O stretching vibration. The 2915 and 2848 $cm^{-1}$ peaks were described as the active stretching and banding vibrations of the $—CH_2$ and $—CH_3$ groups, respectively. The symmetric stretching of the C—C(═O)—O group was observed at 1452 $cm^{-1}$. Peaks at the range of 1500–1150 $cm^{-1}$ correspond to the ester groups in polylactide molecules. The scissor vibration of $\delta_s(—CH_3)$ group and the bending vibration of the $\delta_1(—CH_3)$ group are detected at 1383 $cm^{-1}$ and 1367 $cm^{-1}$. The vibration at 1182 $cm^{-1}$ is related to the ester group (—C—O—).

The SEM images and element distribution mapping of the cross-section of 10-nHAp/PLDLLA composition are presented in Fig. 3. The pictures show a quite homogeneous distribution of nHAp in the composite. The element mapping proves good distribution and negligible agglomeration of the nHAp nanocrystals in the polymeric matrix.

The weight-average molar weight ($M_w$) and number average molecular weight ($M_N$) were evaluated for the pure PLDLLA, 10-nHAp/PLDLLA after the first (mixing and pellet preparation) and the second extrusion (shaping) as well as 20-nHAp/PLDLLA after the first extrusion (Table 1). The dispersity indexes ($D$) were calculated as per Equation (1) as shown in Table 1. Values of average molar weight decrease after the first extrusion process more than twice. The second extrusion also influenced the average molar weight, but the changes were less significant. After the first extrusion process, the $M_N$ of composition 20-nHAp/PLDLLA was lower than that of the 10-nHAp/PLDLLA composition. The $M_N$ considers the presence of low-weight molecules (herein nHAp) which influenced average molecular weight. However, it may be suggested that twice higher wt.% of hydroxyapatite filler does not affect weight loss during the extrusion process.

The pure PLDLLA, as well as nHAp/PLDLLA compositions, were investigated using $^1H$ NMR spectroscopy (see Fig. 4). This technique was used to obtain the structural characterization of the material. The most intense resonances of methyl chain ($H^a$) were detected at 1.61 and at 1.60 ppm. The —CH($CH_3$)- methine chain ($H^b$) as well as end methine

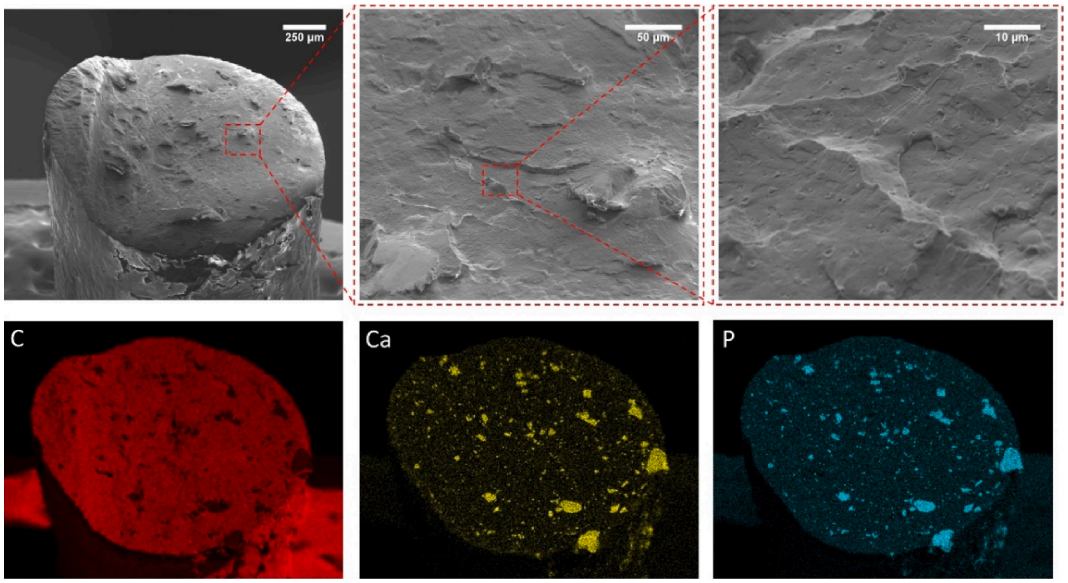


**Fig. 3.** The SEM images (top) and element distribution mapping (bottom) of the 10-nHAp/PLDLLA composition.

**Table 1**
Weight-average molar weight (Mw), number average molecular weight (Mn) and dispersity indexes (D) of the pure PLDLLA and nHAp/PLDLLA compositions.

| Sample | $M_n$ [g/mol] | $M_w$ [g/mol] | $D$ [arb. u.] |
|---|---|---|---|
| PLDLLA PURE (L-lactide-*co*-D,L-lactide copolymer) | 332 800 | 761 300 | 2,29 |
| 10-nHAp/PLDLLA extrusion 1 | 114 800 | 248 000 | 2,16 |
| 10-nHAp/PLDLLA extrusion 2 | 88 900 | 186 500 | 2,09 |
| 20-nHAp/PLDLLA extrusion 1 | 98 000 | 240 500 | 2,45 |

unit ($H^d$) result in a quadruplet at 5.19 ppm. The signal corresponding to the end unit —OH ($H^e$) groups was detected only in case of pure PLDLLA at 2.38 ppm. The signal associated with the end methyl unit ($H^c$) are overlapping with the methyl chain ($H^a$) resonance [35,36]

Thermogravimetric analysis (TGA) was performed to evaluate the influence of nHAp modifier on the thermal stability of PLDLLA and validate the amount of the filler in the composites, i.e., to verify the efficiency of melt mixing of the composites. The TGA curves of PLDLLA and nHAp/PLDLLA sheets recorded upon heating at 10 °C/min and normalized to the initial sample mass are presented in Fig. 5. Pure PLDLLA undergoes a one-stage decomposition process which starts at 340 °C as typically for polylactide materials. Decomposition of PLDLLA progresses due to random or specific chain-end scission and results in a gradual molar mass decrease [6,37–40]. The addition of nHAp to the

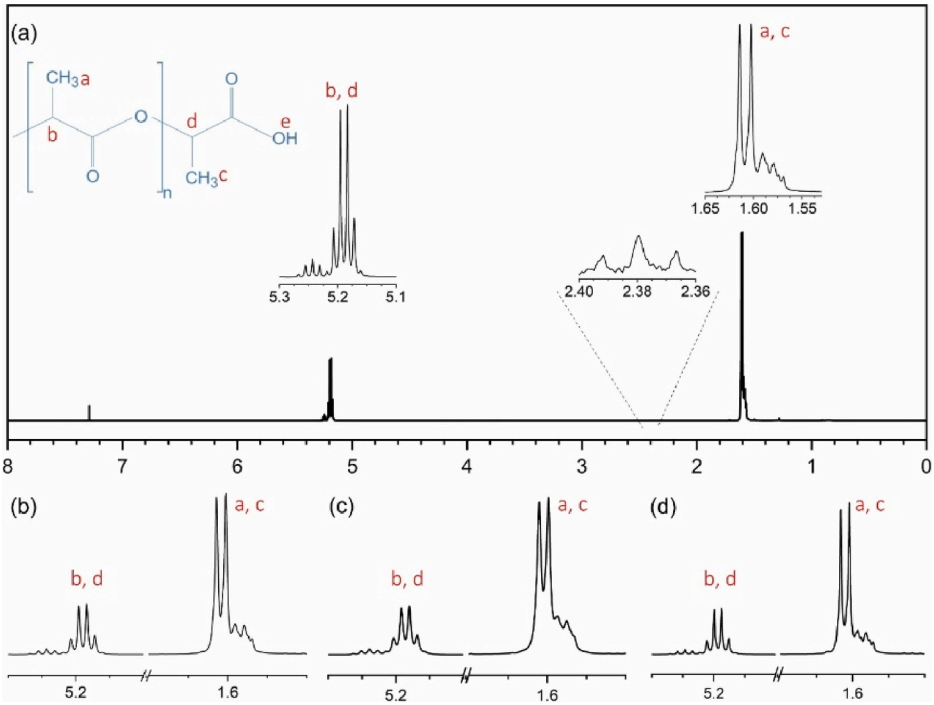


**Fig. 4.** $^1$H NMR spectra of pure PLDLLA (a), 10-nHAp/PLDLLA extrusion 1 (b), 10-nHAp/PLDLLA extrusion 2 (c) as well as 20-nHAp/PLDLLA extrusion 1 (d).

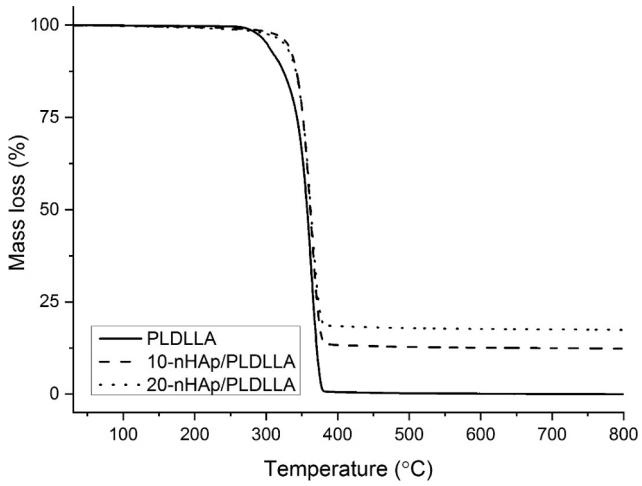


**Fig. 5.** Thermogravimetric curves of PLDLLA and nHAp/PLDLLA composites upon heating at 10 °C $min^{-1}$ in nitrogen atmosphere: mass loss as a function of temperature.

PLDLLA matrix affects the mass-temperature profile leading to thermal stability enhancement as a result of the thermally stable filler in the composition. The higher thermal stability of nHAp/PLDLLA formulations, in comparison to pure PLDLLA, as shown in Fig. 5, results in the onset of mass loss moved towards higher temperatures. This may positively affect further processing as enhanced thermal stability may reduce an average molar mass loss exhibited during the second extrusion (filament formation) and further 3D printing. The filler content seems not to affect the thermal stability of the compositions. Worth noting is that pure PLDLLA decomposes entirely upon the applied temperature profile. The composites reveal higher residual mass values appropriate to the composition. The residual masses of the 10- and 20-nHAp/PLDLLA composites are 12 and 17 %, respectively. Considering the experimental error, which varies within approx. 2 %, it is assumed that the amount of the filler in the compositions agrees with the research plan and proves that the proposed melt mixing procedure is an excellent tool for producing uniform compositions.

Brinell hardness and density were determined to verify an influence of the nHAp modifier on physical properties of the composites. The results are presented in Fig. 6. Pure PLDLLA revealed hardness of approx. 100 HB. An addition of hard ceramic particles of nanosized modifier resulted in an increase of the value up to 135 HB. A similar tendency was evidenced in the case of density values. The incorporation of nHAp resulted in a rise of the value from 1.23 up to 1.38 g/$cm^3$ for the highest filler content. This trend was expected upon the addition of rigid, high-density particles into the PLDLLA matrix. The changes are reflected in the composites' utility properties, resulting in an increased mass of the product and its high solidity. Hence, it ensures sufficient properties to serve as medical implants for orthopedic surgery. Such composites aiming to mimic the composite nature of natural bone combine the polymer phase's toughness with an inorganic filler's compressive strength to generate bioactive material with improved mechanical properties and degradation profile [18].

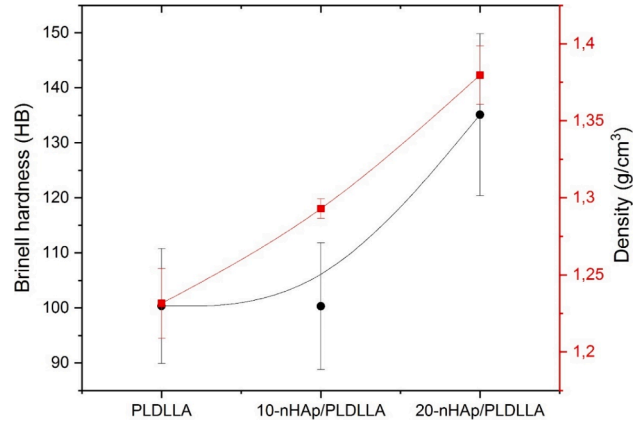


**Fig. 6.** Brinell hardness and density of PLDLLA and nHAp/PLDLLA composites in a function of composition.

Bone implant requires sufficient mechanical strength and must be durable enough to maintain its properties during the implantation procedure. After implementation in the body, it needs to provide short-term mechanical support for the overgrowing bone. Table 2 shows tensile ($\sigma_m$) and flexural strengths ($\sigma_{fm}$), Young's ($E_t$), and flexural ($E_f$) moduli and flexural strain ($\varepsilon_{fm}$) of the composites with various nHAp/PLDLLA ratios upon static and bending tests. It was observed that the $\sigma_m$ and $\sigma_{mf}$ decrease with an increasing amount of nHAp. The flexural strength dropped from 115.0 MPa, for pure PLDLLA, down to 95.7 and 81.4 MPa for the 10- and 20-nHAp/PLDLLA, respectively. Simultaneously, the tensile strength dropped from 41.8 MPa, for the pure matrix, down to 38.6 and 27.4 MPa for the composites, respectively. It is well known that introducing a rigid filler in polylactide decreases the strength of the composite material. Still, on the other hand, it increases the stiffness, as evidenced by enhanced Young's modulus values [23]. From the application point of view, a decrease in bending strength for nHAp/PLDLLA composites, in comparison to unmodified PLDLLA, is desired as the values of $\sigma_{fm}$ become similar to natural cortical bone (61 MPa) [41]. Moreover, a slight increase in the flexural modulus for the nHAp/PLDLLA composites was observed (up to about 1.80 GPa), which is close to the experimental error. An increase in material stiffness results in increased brittleness of the material. Both, $\varepsilon_b$ and $\varepsilon_{fm}$, decrease with the nHAp content, i.e., the elongation at break dropped from 3.1 %, for the pure matrix, down to 2.6 and 1.3 % for the composites, respectively. The flexural strain values decreased from 5.6 %, for the pure PLDLLA, down to 2.7% for the 20-nHAp/PLDLLA. However, it should be noted that this reduction does not discredit the composites as a material with the potential to produce medical implants. On the contrary, it was proved that nHAp/PLDLLA composites have sufficient strength and durability to replace bone defects.

Water and diiodomethane contact angles determined for pure PLDLLA, 10-nHAp/PLDLLA, and 20-HAp/PLDLLA are shown in Fig. 7. It was noted that water contact angles (WCAs) are higher for the 10-nHAp/PLDLLA and 20-nHAp/PLDLLA than for pure PLDLLA, i.e., the surface of the composites is more hydrophobic than pure material. The value of WCA for pure matrix is in agreement with the literature [42]. In recent reports, it has been suggested that biomaterials with water contact angles higher than 65° could be less susceptible to cell adhesion than hydrophilic substrates [43]. On the other hand, the hydrophobic surfaces ($\theta > 90°$) are linked with better cell–cell cohesion. According to these studies and the WCA data in Fig. 7, favored growth of tissue on 10-nHAp/PLDLLA composite is expected. In contrast, the cell-material adhesion should be smaller than for pure PLDLLA and 20-nHAp/PLDLLA. The values of diiodomethane contact angles are slightly higher for composites than for PLDLLA. It means that nonpolar liquids

**Table 2**
Tensile strength ($\sigma_m$), flexural strength ($\sigma_{fm}$), Young's modulus ($E_t$), flexural modulus ($E_f$), elongation at break ($\varepsilon_b$), and flexural strain ($\varepsilon_{fm}$) of the pure PLDLLA and nHAp/PLDLLA compositions.

| Sample | $\sigma_m$ [MPa] | $\sigma_{fm}$ [MPa] | $E_t$ [GPa] | $E_f$ [GPa] | $\varepsilon_b$ [%] | $\varepsilon_{fm}$ [%] |
|---|---|---|---|---|---|---|
| PLDLLA | 41.8 ± 11.8 | 115 ± 10.2 | 2.1 ± 0.0 | 1.70 ± 0.13 | 3.1 ± 1.1 | 5.6 ± 0.61 |
| 10-nHAp/PLDLLA | 38.6 ± 5.4 | 95.7 ± 8.7 | 2.1 ± 0.2 | 1.82 ± 0.27 | 2.6 ± 0.6 | 3.7 ± 0.04 |
| 20-nHAp/PLDLLA | 27.4 ± 13.3 | 81.4 ± 5.5 | 2.6 ± 0.3 | 1.83 ± 0.03 | 1.3 ± 0.6 | 2.7 ± 0.10 |

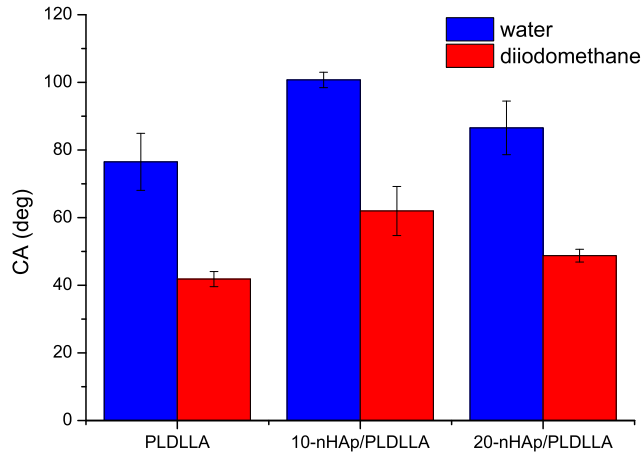


**Fig. 7.** Average water and diiodomethane contact angles determined for pure PLDLLA, 10-nHAp/PLDLLA, and 20-nHAp/PLDLLA.

possess higher affinity to the surface of nHAp/PLDLLA than to pure polylactide. However, contact angle alone is not sufficient to the cell-surface interaction as the cell response to a biomaterial is much more complex.

The surface free energy (SFE) is a thermodynamic quantity that interprets phenomena occurring at the interface. In the case of biomedical materials, it reflects their biological response. Here, the surface free energy was calculated as per Eq. (3) using the contact angle data for PLDLLA and compression-molded composites, as shown in Table 3.

The role of SFE in the biocompatibility of materials related to bone implants has already been recognized in terms of cell adhesion including bacteria and osteoblasts. The SFE value for ideal cell spreading and growth has been indicated as 57 $mJ \cdot m^{-2}$, close to the result obtained for pure PLDLLA [44]. Other reports indicate that the real contribution of surface free energy to protein adsorption and cell adhesion is not fully understood [45]. Nevertheless, every change in SFE affects cell behavior. In our study, the total surface free energy of PLDLLA (55.57 $mJ \cdot cm^{-2}$) was reduced through compositional changes to 39.74 and 50.13 $mJ \cdot cm^{-2}$, respectively. The dispersive component of the SFE was modified in contrast to the polar part which remained relatively high for nHAp/PLDLLA. The differences in the SFEs may be crucial for adsorption and conformation of proteins and their distribution across the surface of PLDLLA-based composites [46]. The addition of hydroxyapatite to the polymer matrix improves the surface topology of the material by enhancing the specific surface area leading to increased material-protein interactions, enhanced cell adhesion, as well as cell proliferation and differentiation [16,47,48]. The proteins are more likely to form separated island-like structures on lower surface free energy surface (herein 10-nHAp/PLDLLA), while higher SFE favors the formation of reticulated structures. Therefore, the differences in SFE of PLDLLA and nHAp/PLDLLA composites may affect the morphology of protein layers built on their surfaces. The results provide the first indication of the suitability of the nHAp/PLDLLA composites for application as regenerative materials in bone surgery. However, the other factors must also be considered in each specific application, e.g., the protein chemistry, including its hydrophilic/hydrophobic nature and surface roughness.

**Table 3**
Total surface free energy values and its components calculated according to the OWRK approach for pure PLDLLA, 10-nHAp/PLDLLA, and 20-nHAp/PLDLLA composites.

| | PLDLLA | 10-nHAp/PLDLLA | 20-nHAp/PLDLLA |
|---|---|---|---|
| SFE [$mJ \cdot cm^{-2}$] | 55.57 | 39.74 | 50.13 |
| $\gamma Sd$ | 19.33 | 8.41 | 14.28 |
| $\gamma Sp$ | 36.24 | 31.33 | 35.85 |

### 3.1. Bacterial adhesion

The ability of bacterial strains forming biofilm was evaluated on both samples (10-nHAp/PLDLLA and 20-nHAp/PLDLLA). It can be noted that the yellowish, green and red particles were detected in all microscopic images (see Fig. 8) also in the control ones (without bacteria). It could be assumed that the observed objects are the agglomerated hydroxyapatite particles. Moreover, no emission was detected in the composition without Syto 9 and propidium iodide addition. This observation provides that these objects could be visualized due to the interaction between hydroxyapatite and fluorescent dyes. The emission of hydroxyapatite excited at different wavelengths was broadly described by Machado et al. [49]. Furthermore, the microscopic images (see Fig. 8) suggest that bacterial adhesion and biofilm formation on both types of materials (10-nHAp/PLDLLA and 20-nHAp/PLDLLA) are comparable. Most of the tested strains cannot form mature biofilm structures on the nHAp-filled material surfaces, and only single adhered living cells (green) are spotted. The mature biofilms were created only by *S. epidermidis* and *P. aeruginosa*. However, it is likely due to their naturally high tendency to produce biofilms which cannot be seen in other strains [50,51].

Previously, the conducted research also describes the ability of bacterial strains to form biofilm on the surface of PLA-based hydroxyapatite-loaded materials. In the work of Woźna et al. (2018) the high adhesion of *P. aeruginosa* cells was also described as well as of *S. aureus* strain. Moreover, the authors proved that the amount of the adhered cells increased with an increase of hydroxyapatite content (20 and 30%) [52]. The other polymers were previously tested as well: poly (orthoester) (POE), polysulfone (PSF), polyethylene (PE), and poly (ether ether ketone) (PEEK) [53] and the bacterial adhesion was evaluated for *P. aeruginosa*, *E. coli* and *S. epidermidis*. The large number of the adhered cells were spotted on all tested polymers. However, the differences between particular strains were observed. Interestingly, *S. epidermidis* was the least adherent among tested bacteria what contradicts with our results. However, the author used different strain (*S. epidermidis* ATCC 12228) so an exact comparison is not possible [53].

## 4. Conclusions

Fully bioresorbable PLDLLA filled with nanohydroxyapatite composites were prepared *via* melt mixing in various formulations (10 and 20 wt%), and described in the mechanical, physicochemical as well as bacterial properties. The performed X-ray and FT-IR analysis proved the efficient procedure of nHAp synthesis and its incorporation into the PLDLLA matrix *via* extrusion. An influence of further processing methods on average molar mass was investigated using gel permeation chromatography which proved the decrease of the polymer chain length. The phenomenon is the most evident in the first extrusion (mixing of ingredients) and less significant during the second one aiming at the filament formation for further 3D printing technology. Thermogravimetric analysis indicated enhanced thermal stability upon nHAp modification. Moreover, the amount of residual mass proved (together with SEM analysis) proper distribution of the filler in the polymeric matrix. Also, mechanical properties improved upon the filler addition with resulting bending strength and density values similar to natural cortical bone. Therefore, the implant produced of such a material would be characterized with low mass, which is comparable to the human bone and twice lower than its titanium counterpart.

Contact angle measurements proved favored growth of tissue on 10-nHAp/PLDLLA sample which agreed with the results of the bacterial adhesion. These outcomes demonstrate that nHAp incorporation is desired due to enhanced bioactivity, thermal, mechanical, and structural properties. However, its amount should be optimized to balance the above properties and susceptibility related to biofilm formation.

Summing up, this kind of the novel and reinforced material composed of PLDLLA and nHAp nanoparticles can be utilized as internal

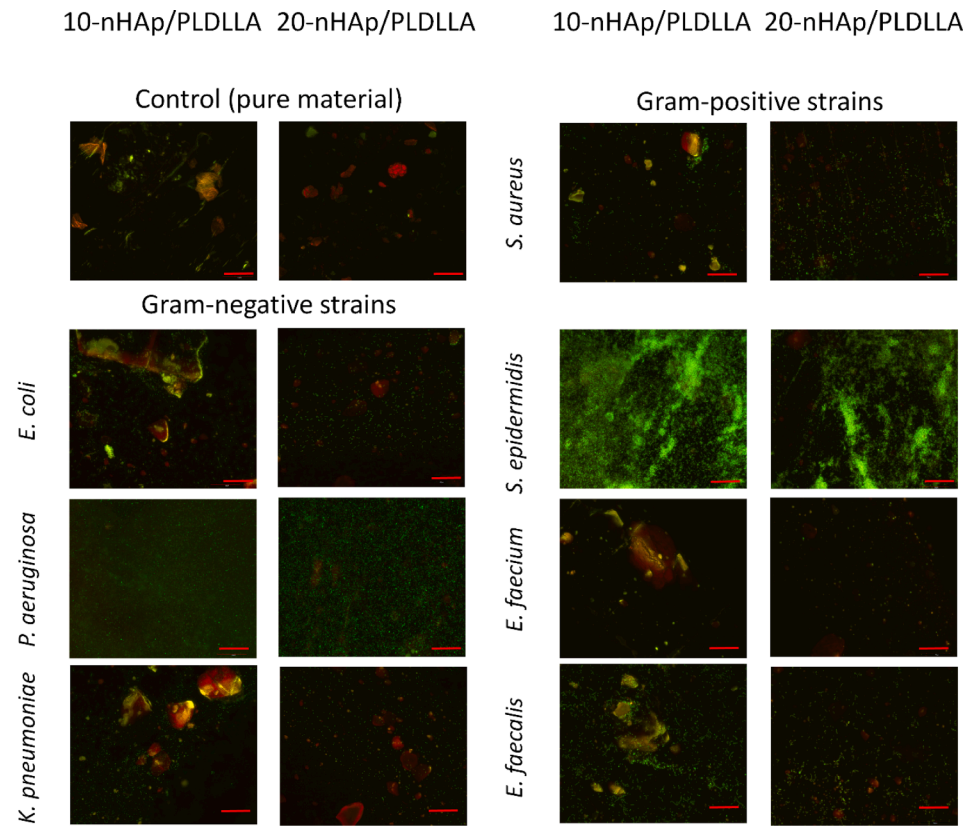


**Fig. 8.** Selected bacterial biofilm on the surfaces of 10-nHAp/PLDLLA and 20-nHAp/PLDLLA) (scale bar = 50 μm).

bone fixation implants in many medical fields, including orthopedic, oral, maxillofacial, craniofacial, as well as plastic and reconstructive surgeries. Its excellent usefulness to these purposes is supported not only by the material superior mechanical properties but also by its bioactivity and complete resorbability. Our biomaterial has already been embedded into the human skull which will be shown in our forthcoming manuscript.

## Funding

The authors would like to acknowledge the National Science Centre, Poland (NCN) for financial support within the project "Preparation and characterisation of biocomposites based on nanoapatites for theranostics" (No. UMO-2015/19/B/ST5/01330) as well as the National Centre for Research and Development with the project "Development of customized biodegradable implants for bone reconstruction procedures" which was carried out under the Operational Programme Smart Growth 2014–2020, agreement no. POIR.01.01.01–00-0646/19–00 with The National Centre for Research and Development, co-financed by the European Regional Development Fund (ERDF) under supervision of Syntplant sp. z o.o. (Poland). The research was also supported by Poznan University of Technology under the project no. 0613/SBAD/4710.

## Declaration of Competing Interest

The authors declare that they have no known competing financial interests or personal relationships that could have appeared to influence the work reported in this paper.

## Acknowledgement

We are grateful to M.Sc. E. Bukowska for XRD measurements, to Ph. D. D. Szymanski for SEM-EDS imaging, to Prof. Z. Drulis-Kawa and Ph.D. A. Piecuch for sharing bacterial strains.

## References

[1] K.R. Mohamed, H.H. Beherei, Z.M. El-Rashidy, In vitro study of nano-hydroxyapatite/chitosan-gelatin composites for bio-applications, J. Adv. Res. 5 (2014) 201–208, https://doi.org/10.1016/j.jare.2013.02.004.
[2] X. Niu, Q. Feng, M. Wang, X. Guo, Q. Zheng, Porous nano-HA/collagen/PLLA scaffold containing chitosan microspheres for controlled delivery of synthetic peptide derived from BMP-2, J. Control. Release 134 (2009) 111–117, https://doi.org/10.1016/j.jconrel.2008.11.020.
[3] X. Peng, Y. Zhang, Y. Chen, S. Li, B. He, Synthesis and crystallization of well-defined biodegradable miktoarm star PEG-PCL-PLLA copolymer, Mater. Lett. 171 (2016) 83–86, https://doi.org/10.1016/j.matlet.2016.02.057.
[4] D.J. Hickey, B. Ercan, L. Sun, T.J. Webster, Adding MgO nanoparticles to hydroxyapatite-PLLA nanocomposites for improved bone tissue engineering applications, Acta Biomater. 14 (2015) 175–184, https://doi.org/10.1016/j.actbio.2014.12.004.
[5] M. Cocca, M.L. Di Lorenzo, M. Malinconico, V. Frezza, Influence of crystal polymorphism on mechanical and barrier properties of poly(l-lactic acid), Eur. Polym. J. 47 (2011) 1073–1080, https://doi.org/10.1016/j.eurpolymj.2011.02.009.
[6] M. Dobrzyńska-Mizera, M. Knitter, S. Mallardo, M.C. Del Barone, G. Santagata, M. L. Di Lorenzo, Thermal and thermo-mechanical properties of poly(L-lactic acid) biocomposites containing β-cyclodextrin/d-limonene inclusion complex, Materials (Basel). 14 (2021) 2569, https://doi.org/10.3390/ma14102569.
[7] Synthesis, Structure and Properties of Poly(lactic acid), in: M.L. Di Lorenzo, R. Androsch, (Eds.), Advances in Polymer Science, Vol. 279, Springer International Publishing, Cham, 2018, ISBN 978-3-319-64229-1.
[8] M.L. Di Lorenzo, R. Androsch, Industrial Applications of Poly(lactic acid), in: M.L. Di Lorenzo, R. Androsch, (Eds.), Advances in Polymer Science, Vol. 282, Springer International Publishing, Cham, 2018, ISBN 978-3-319-75458-1.
[9] T. Kanno, S. Sukegawa, Y. Furuki, Y. Nariai, J. Sekine, Overview of innovative advances in bioresorbable plate systems for oral and maxillofacial surgery, Jpn. Dent. Sci. Rev. 54 (2018) 127–138, https://doi.org/10.1016/j.jdsr.2018.03.003.
[10] P. Schumann, D. Lindhorst, M.E.H. Wagner, A. Schramm, N.-C. Gellrich, M. Rücker, Perspectives on resorbable osteosynthesis materials in craniomaxillofacial surgery, Pathobiology 80 (2013) 211–217, https://doi.org/10.1159/000348328.
[11] H. Pihlajamaki, O. Bostman, E. Hirvensalo, P. Tormala, P. Rokkanen, Absorbable pins of self-reinforced poly-L-lactic acid for fixation of fractures and osteotomies, J. Bone Joint Surg. Br. 74-B (1992) 853–857, https://doi.org/10.1302/0301-620X.74B6.1447246.

[12] S. Sukegawa, T. Kanno, D. Nagano, A. Shibata, Y. Sukegawa-Takahashi, Y. Furuki, The clinical feasibility of newly developed thin flat-type bioresorbable osteosynthesis devices for the internal fixation of zygomatic fractures, J. Craniofac. Surg. 27 (2016) 2124–2129, https://doi.org/10.1097/SCS.0000000000003147.
[13] J. Bergsma, Late degradation tissue response to poly(?-lactide) bone plates and screws, Biomaterials 16 (1995) 25–31, https://doi.org/10.1016/0142-9612(95)91092-D.
[14] E.J. Bergsma, F.R. Rozema, R.R.M. Bos, W.C.D. Bruijn, Foreign body reactions to resorbable poly(l-lactide) bone plates and screws used for the fixation of unstable zygomatic fractures, J. Oral Maxillofac. Surg. 51 (1993) 666–670, https://doi.org/10.1016/S0278-2391(10)80267-8.
[15] F.S. Senatov, K.V. Niaza, M.Y. Zadorozhnyy, A.V. Maksimkin, S.D. Kaloshkin, Y. Z. Estrin, Mechanical properties and shape memory effect of 3D-printed PLA-based porous scaffolds, J. Mech. Behav. Biomed. Mater. 57 (2016) 139–148, https://doi.org/10.1016/j.jmbbm.2015.11.036.
[16] M. Persson, G.S. Lorite, H.E. Kokkonen, S.-W. Cho, P.P. Lehenkari, M. Skrifvars, J. Tuukkanen, Effect of bioactive extruded PLA/HA composite films on focal adhesion formation of preosteoblastic cells, Colloids Surf. B Biointerf. 121 (2014) 409–416, https://doi.org/10.1016/j.colsurfb.2014.06.029.
[17] A. Zimina, F. Senatov, R. Choudhary, E. Kolesnikov, N. Anisimova, M. Kiselevskiy, P. Orlova, N. Strukova, M. Generalova, V. Manskikh, et al., Biocompatibility and physico-chemical properties of highly porous PLA/HA scaffolds for bone reconstruction, Polymers (Basel). 12 (2020) 2938, https://doi.org/10.3390/polym12122938.
[18] I. Armentano, M. Dottori, E. Fortunati, S. Mattioli, J.M. Kenny, Biodegradable polymer matrix nanocomposites for tissue engineering: a review, Polym. Degrad. Stab. 95 (2010) 2126–2146, https://doi.org/10.1016/j.polymdegradstab.2010.06.007.
[19] S. Targonska, R.J. Wiglusz, Investigation of physicochemical properties of the structurally modified nanosized silicate-substituted hydroxyapatite co-doped with Eu3+ and Sr2+ ions, Nanomaterials 11 (2020) 27, https://doi.org/10.3390/nano11010027.
[20] F. Ridi, I. Meazzini, B. Castroflorio, M. Bonini, D. Berti, P. Baglioni, Functional calcium phosphate composites in nanomedicine, Adv. Colloid Interface Sci. 244 (2017) 281–295.
[21] S.L. Aktuğ, S. Durdu, E. Yalçın, K. Çavuşoğlu, M. Usta, Bioactivity and biocompatibility of hydroxyapatite-based bioceramic coatings on zirconium by plasma electrolytic oxidation, Mater. Sci. Eng. C 71 (2017) 1020–1027, https://doi.org/10.1016/j.msec.2016.11.012.
[22] C.R. Rocha, D. Chávez-Flores, N. Zuverza-Mena, A. Duarte, B.A. Rocha-Gutiérrez, E.A. Zaragoza-Contreras, S. Flores-Gallardo, Surface organo-modification of hydroxyapatites to improve <scp>PLA</scp> / <scp>HA</scp> compatibility, J. Appl. Polym. Sci. 137 (2020) 49293, https://doi.org/10.1002/app.49293.
[23] V.A. Demina, S.V. Krasheninnikov, A.I. Buzin, R.A. Kamyshinsky, N.V. Sadovskaya, E.N. Goncharov, N.A. Zhukova, M.V. Khvostov, A.V. Pavlova, T.G. Tolstikova, et al., Biodegradable poly(l-lactide)/calcium phosphate composites with improved properties for orthopedics: Effect of filler and polymer crystallinity, Mater. Sci. Eng. C 112 (2020), 110813, https://doi.org/10.1016/j.msec.2020.110813.
[24] S.S. Sharifabad, H.A. Derazkola, M. Esfandyar, M. Elyasi, F. Khodabakhshi, Mechanical properties of HA@Ag/PLA nanocomposite structures prepared by extrusion-based additive manufacturing, J. Mech. Behav. Biomed. Mater. 118 (2021), 104455, https://doi.org/10.1016/j.jmbbm.2021.104455.
[25] G. Narayanan, V.N. Vernekar, E.L. Kuyinu, C.T. Laurencin, Poly (lactic acid)-based biomaterials for orthopaedic regenerative engineering, Adv. Drug Deliv. Rev. 107 (2016) 247–276, https://doi.org/10.1016/j.addr.2016.04.015.
[26] M. Gimeno, P. Pinczowski, M. Pérez, A. Giorello, M.Á. Martínez, J. Santamaría, M. Arruebo, L. Luján, A controlled antibiotic release system to prevent orthopedic-implant associated infections: an in vitro study, Eur. J. Pharm. Biopharm. 96 (2015) 264–271, https://doi.org/10.1016/j.ejpb.2015.08.007.
[27] C.R. Arciola, D. Campoccia, L. Montanaro, Implant infections: adhesion, biofilm formation and immune evasion, Nat. Rev. Microbiol. 16 (2018) 397–409, https://doi.org/10.1038/s41579-018-0019-y.
[28] M. Dobrzyńska-Mizera, M. Knitter, A. Woźniak-Braszak, M. Baranowski, T. Sterzyński, M.L. Di Lorenzo, Poly(L-lactic acid)/pine wood bio-based composites, Materials (Basel). 13 (2020) 3776, https://doi.org/10.3390/MA13173776.
[29] PN-EN_ISO527-1 Organisation Internationale de Normalisation. Plastics—Determination of Tensile Properties—Part 1: General Principles, 2012.
[30] PN-EN_ISO 178:2019-06 Tworzywa sztuczne – Oznaczanie właściwości przy zginaniu, 2019.
[31] PN-EN_ISO_2039-1, Tworzywa sztuczne – Oznaczanie twardości – Część 1: Metoda wciskania kulki, 2004.
[32] PN-EN_ISO 1183-1:2019-05 Tworzywa sztuczne – Metody oznaczania gęstości tworzyw sztucznych nieporowatych – Część 1: Metoda zanurzeniowa, metoda piknometru cieczowego i metoda miareczkowa.
[33] D.K. Owens, R.C. Wendt, Estimation of the surface free energy of polymers, J. Appl. Polym. Sci. 13 (1969) 1741–1747, https://doi.org/10.1002/app.1969.070130815.
[34] S. Liu, Y. Zheng, R. Liu, C. Tian, Preparation and characterization of a novel polylactic acid/hydroxyapatite composite scaffold with biomimetic micro-nanofibrous porous structure, J. Mater. Sci. Mater. Med. 31 (2020) 74, https://doi.org/10.1007/s10856-020-06415-4.
[35] E. Olewnik-Kruszkowska, I. Koter, J. Skopińska-Wiśniewska, J. Richert, Degradation of polylactide composites under UV irradiation at 254 nm, J. Photochem. Photobiol. A Chem. 311 (2015) 144–153, https://doi.org/10.1016/j.jphotochem.2015.06.029.
[36] E. Olewnik, W. Czerwiński, J. Nowaczyk, M.-O. Sepulchre, M. Tessier, S. Salhi, A. Fradet, Synthesis and structural study of copolymers of l-lactic acid and bis(2-hydroxyethyl terephthalate), Eur. Polym. J. 43 (2007) 1009–1019, https://doi.org/10.1016/j.eurpolymj.2006.11.025.
[37] C. Zeng, N.-W. Zhang, S.-Q. Feng, J. Ren, Thermal stability of copolymer derived from l-lactic acid and poly(tetramethylene) glycol through direct polycondensation, J. Therm. Anal. Calorim. 111 (2013) 633–646, https://doi.org/10.1007/s10973-012-2542-9.
[38] M.L. Di Lorenzo, R. Ovyn, M. Malinconico, P. Rubino, Y. Grohens, Peculiar crystallization kinetics of biodegradable poly(lactic acid)/poly(propylene carbonate) blends, Polym. Eng. Sci. 55 (2015) 2698–2705, https://doi.org/10.1002/pen.24058.
[39] M.L. Di Lorenzo, A. Longo, N, N-Diethyl-3-methylbenzamide (DEET): a mosquito repellent as functional plasticizer for poly(l-lactic acid), Thermochim. Acta 677 (2019) 180–185, https://doi.org/10.1016/j.tca.2019.02.004.
[40] A. Södergård, J.H. Näsman, Melt stability study of various types of poly(<scp>l</scp> -lactide), Ind. Eng. Chem. Res. 35 (1996) 732–735, https://doi.org/10.1021/ie950338f.
[41] S. Sadudeethanakul, W. Wattanutchariya, W. Nakkiew, A. Chaijaruwanich, S. Pitjamit, Bending strength and Biological properties of PLA-HA composites for femoral canine bone fixation plate, IOP Conf. Ser. Mater. Sci. Eng. 635 (2019), 012004, https://doi.org/10.1088/1757-899X/635/1/012004.
[42] A. Rapacz-Kmita, M.K. Pierchała, A. Tomas-Trybuś, B. Szaraniec, J. Karwot, The wettability, mechanical and antimicrobial properties of polylactide/montmorillonite nanocomposite films, Acta Bioeng. Biomech. 19 (2017) 25–33, https://doi.org/10.5277//ABB-00820-2017-02.
[43] R. Tzoneva, N. Faucheux, T. Groth, Wettability of substrata controls cell-substrate and cell-cell adhesions, Biochim. Biophys. Acta - Gen. Subj. 1770 (2007) 1538–1547, https://doi.org/10.1016/j.bbagen.2007.07.008.
[44] J.M. Schakenraad, H.J. Busscher, C.R.H. Wildevuur, J. Arends, The influence of substratum surface free energy on growth and spreading of human fibroblasts in the presence and absence of serum proteins, J. Biomed. Mater. Res. 20 (1986) 773–784, https://doi.org/10.1002/jbm.820200609.
[45] M.M. Gentleman, E. Gentleman, The role of surface free energy in osteoblast–biomaterial interactions, Int. Mater. Rev. 59 (2014) 417–429, https://doi.org/10.1179/1743280414Y.0000000038.
[46] J.A. Nychka, M.M. Gentleman, Implications of wettability in biological materials science, JOM 62 (2010) 39–48, https://doi.org/10.1007/S11837-010-0107-6.
[47] G. Sui, X. Yang, F. Mei, X. Hu, G. Chen, X. Deng, S. Ryu, Poly-L-lactic acid/hydroxyapatite hybrid membrane for bone tissue regeneration, J. Biomed. Mater. Res. - Part A 82 (2007) 445–454, https://doi.org/10.1002/jbm.a.31166.
[48] K. Rechendorff, M.B. Hovgaard, M. Foss, V.P. Zhdanov, F. Besenbacher, Enhancement of protein adsorption induced by surface roughness, Langmuir 22 (2006) 10885–10888, https://doi.org/10.1021/la0621923.
[49] T.R. Machado, I.S. Leite, N.M. Inada, M.S. Li, J.S. da Silva, J. Andrés, H. Beltrán-Mir, E. Cordoncillo, E. Longo, Designing biocompatible and multicolor fluorescent hydroxyapatite nanoparticles for cell-imaging applications, Mater. Today Chem. 14 (2019), 100211, https://doi.org/10.1016/j.mtchem.2019.100211.
[50] M. Pihl, L.E. Chávez de Paz, A. Schmidtchen, G. Svensäter, J.R. Davies, Effects of clinical isolates of Pseudomonas aeruginosa on Staphylococcus epidermidis biofilm formation, FEMS Immunol. Med. Microbiol. 59 (2010) 504–512, https://doi.org/10.1111/j.1574-695X.2010.00707.x.
[51] W. Hou, X. Sun, Z. Wang, Y. Zhang, Biofilm-forming capacity of staphylococcus epidermidis, staphylococcus aureus, and pseudomonas aeruginosa from ocular infections, Investig. Opthalmology Vis. Sci. 53 (2012) 5624, https://doi.org/10.1167/iovs.11-9114.
[52] A.E. Woźna, A.F. Junka, P.E. Szymczyk, The influence of different composite mixtures (PLA/HA) manufactured with additive laser technology on the ability of S. aureus and P. aeruginosa to form biofilms, Acta Bioeng. Biomech. Orig. Pap. 20 (2018), https://doi.org/10.5277/ABB-01135-2018-02.
[53] A.J. Barton, R.D. Sagers, W.G. Pitt', Bacterial adhesion to orthopedic implant polymers, J. Biomed. Mater. Res. 30 (1996) 403–410, https://doi.org/10.1002/(SICI)1097-4636(199603)30:3.